**Earthquakes and Structures**, *Vol. 7, No. 6 (2014) 909-935*
DOI: http://dx.doi.org/10.12989/eas.2014.7.6.909 

# Performance of retaining walls with and without sound wall under seismic loads

Erin Mock[1] and Lijuan Cheng[*2]

[1]*Alta Vista Solutions, Inc., 3260 Blume Dr., Suite 500, Richmond, CA 94806, U.S.A*
[2]*Department of Civil and Environmental Engineering, University of California, Davis, One Shields Ave., Davis, CA 95616, U.S.A*

*(Received May 9, 2014, Revised May 21, 2014, Accepted May 21, 2014)*

**Abstract.** The seismic characteristics of two semi-gravity reinforced concrete cantilever retaining walls are examined via an experimental program using an outdoor shake table (one with and the other without concrete masonry sound wall on top). Both walls are backfilled with compacted soil and supported on flexible foundation in a steel soil container. The primary damages during both tests are associated with significant lateral displacements of the wall caused by lateral earth pressure; however, no collapse occurs during the tests. The pressure distribution behind the walls has a nonlinear trend and conventional methods such as Mononobe-Okabe are insufficient for accurate pressure estimation.

**Keywords:** retaining wall; sound wall; shake table test; seismic loads; earth pressure

## 1. Introduction

Many public and private sectors have practiced the routine design of retaining walls for static applications, following the codes that are based on simplistic analyses (e.g., Caltrans 2008, CDOT 2009). One of the key design components is the estimation of the active lateral earth pressure behind the wall. Under seismic conditions, calculating lateral earth pressure becomes more challenging and difficult due to the combination of factors such as wall configuration, foundation support, site condition and nonlinear soil-wall interaction. One existing method for modeling seismic pressures is the well-known Mononobe-Okabe (M-O) method (Mononobe and Matsuo 1929). The M-O method is based on a pseudo-static analysis of seismic earth pressures using static Coulomb theory, and is one of the most widely used force-based methods. It is assumed the wall is free to yield sufficiently to enable the full soil strength or active pressure conditions to be mobilized, which typically requires a relatively small wall displacement. Although many researchers and practitioners believe the M-O method provides accurate values (Bolton and Steedman 1982, Fang *et al.* 2003, Ortiz *et al.* 1983, Seed and Whitman 1970), others have argued it gives conservative estimates of earth pressure on the wall, especially for higher intensity

*Corresponding author, Associate Professor, E-mail: dawcheng@ucdavis.edu


 ISSN: 2092-7614 (Print), 2092-7622 (Online)

motions (Al Atik and Sitar 2007, Dewoolkar *et al.* 2001, Stadler 1996). Richard and Elms (1979) discussed the drawback of these simple estimates, given that the method does not consider the effects of wall inertia, which could lead to underestimation of the total force on the wall. Suggestions on accounting for these effects have been proposed (Bolton and Steedman 1982, 1985) as a supplement to the M-O method. Seed and Whitman (1970) point out that the M-O method gives the total force acting on the wall but not necessarily the distribution of lateral pressure on the wall. The location of the resultant force depends on the magnitude and direction of wall movement. Furthermore, the M-O method has been found to have inherent limitations such that it is valid only for non-cohesive soils with no presence of water table (Kramer 1996). Shortcomings and limitations of this method may be exposed further when the backfill slope is greater than 15° and/or the horizontal acceleration coefficient is more than 0.3g (Tavatli and Li 2007).

To overcome the limitations of the M-O method, an alternative design method has been sought for retaining walls. The Newmark method is a displacement-based method and also known as the Newmark sliding block method (AASHTO 2005). The Newmark's sliding block-on-a-plane model can be used to model the permanent deformation resulting from internal and external sliding, and sliding between the facing units. This method, however, still relies on a pseudo-static analysis, and the failure surface exhibits a rigid perfectly plastic shearing behavior (Newmark 1965). As recommended by the AASHTO design guide (AASHTO 2005), this approach shall not be used on retaining walls with complex geometry or where peak accelerations exceed 0.3g. Managing difficulties in the M-O method, such as the high acceleration and large back-slope angle limitations, has been further attempted in a recent study by Anderson *et al.* (2009), where a numerical procedure using the limit-equilibrium stability principle was applied.

To better understand the seismic behavior of retaining walls under earthquake excitations, experimental investigations have also been performed using either centrifuge test or shake table model test (mostly 1g). The centrifuge test can reproduce the stress conditions in the soil more accurately than the 1g model tests, but does not allow extensive instrumentation on small models and the scaling is often complicated. Recent studies using centrifuge tests include those by (Ortiz *et al.* (1983), Al Atik and Sitar (2007), Ortiz (1982), Kutter *et al.* (1990), Siddharthan *et al.* (2004), Ling *et al.* (2004). On the other hand, shake table tests offer the advantage of relatively larger model sizes near prototype-scale soil with real reinforcing materials; however, it cannot simulate the high stresses existing in tall slopes. Such examples include Seed and Whitman (1970) and Ling (2003), where shake table tests were conducted on small-scale model specimens (i.e., with a maximum height of 1 m) under sinusoidal excitations. The effects of scale, stress-levels, and modified soil conditions may not accurately represent the full-scale performance of the on-site retaining wall during real earthquake shaking. Tajiri *et al.* (1996) conducted a full-scale shake table test on 6-m high geotextile-reinforced soil walls with different facing materials (i.e., concrete panels and blocks, expanded polystyrol blocks). More recently, Ling *et al.* (2005) tested three full-scale 2.8-m high modular-block walls reinforced with polymeric geogrids and backfilled with sand in Japan as a benchmark for validating the analytical procedures developed in a separate study. One of their major test results revealed that the design method based on the 1996 AASHTO and National Concrete Masonry Association design resources underestimated the seismic capacity of flexible wall systems (Ling *et al.* 2005). However, full-scale experimental research on retaining walls using shake-table tests is extremely limited in the current literature. In addition, many existing retaining walls also carry a sound wall structure on the top, e.g., masonry block sound

wall connected to the top of the retaining wall (Caltrans 2008). The existence of the sound wall structure affects the dynamic characteristics of the retaining wall-soil structure, the influence of which needs to be incorporated carefully into the seismic design of retaining walls. A performance database is desirable and much needed for the purpose of validating numerical procedures and design methods, and for the reduced-scale physical models in other case studies.

This paper presents the experimental results of two full-scale semi-gravity retaining walls according to the current design practice in California (Caltrans, 2008). The walls are identical except that one wall supports a concrete masonry sound wall on the top. Both walls are backfilled with compacted soil on one side and supported on flexible foundation in a steel soil-container fixed on the shake table. Each soil-wall system is then subjected to a series of unidirectional seismic excitations with wall displacement, dynamic lateral earth pressure, and backfill failure modes recorded. The information allows comparisons to be made with conventional predictions such as the Mononobe-Okabe method, all of which presently appear to lack experimental validation. This study also provides insightful information for numerical modeling and demonstrates the need to re-assess current seismic design standards and specifications.

## 2. Experimental investigation

The experiment was conducted at the NEESR Large High-Performance Outdoor Shake Table at the Englekirk Structural Engineering Center of the University of California, San Diego (NEESR 2012). This facility houses the largest outdoor shake table in the world. The dimensions of the table are 12.2 m (40 ft) in length and 7.6 m (25 ft) in width. The shake table has the capacity to produce motions in the uniaxial direction with a maximum acceleration of 3g, a maximum velocity of 1.8 m/s, and a maximum displacement of 0.75 m (Restrepo *et al.* 2005). The experiment in this study only utilized shake in the uniaxial direction, normal to the face of the retaining walls.

### *2.1 Test specimens*

Two separate tests were conducted on the shake table. The first test consisted of a semi-gravity reinforced concrete cantilever wall backfilled with soil. The second test had the same retaining wall and backfills as in the first test and a concrete masonry sound wall installed on top of the retaining wall. These retaining walls, including the dimensions and rebar layout, were designed according to typical design plans in the Caltrans bridge standard detail sheets (Caltrans, 2008). As shown in Fig. 1, the retaining walls are 2.36 m (7.75 ft) wide and 2.21 m (7.25 ft) high, including the height of the stem and footing. The length of the wall is 2.69 m (8.83 ft), and the thickness of the stem is 0.30 m (1 ft). The sound wall in the second test is 1.83 m (6 ft) high and 2.64 m (8.67 ft) long [Fig. 1(b)]. The thickness of the sound wall is 0.20 m (8 in), which is typical for standard normal weight concrete masonry blocks. Steel reinforcing bars are used to connect the sound wall to the retaining wall, with the bars embedded 0.74 m into the retaining wall and extended to the top of the masonry sound wall.

### *2.2 Materials*

Two batches of concrete pouring were involved in the retaining wall construction: one for the

footing and the other for the stem. The average 28-day compressive strength of concrete for the footing and the stem were 34.6 MPa and 31.4 MPa, respectively, according to ASTM Standard C39/C39M (ASTM 2005a). No. 16 steel reinforcing rebar was used for both retaining walls and the average yielding strength of the rebar was 456 MPa, per ASTM A370 (ASTM 2005b).

The sound wall was constructed from concrete masonry blocks, rebars, grout, and mortar. The masonry blocks were medium weight Grade N concrete masonry unit (CMU) blocks for below and above ground that could be exposed to weather. The CMU block had the strength of 13.8 MPa conforming to ASTM C90 (ASTM 2005c). The mortar used to bond the CMU blocks together was classified as Type S mortar, common for exterior or interior use, and had a compressive strength of 10.3 MPa based on ASTM C270 (ASTM 2005d). The grout that was pumped into the hollow sections of the CMU blocks had a compressive strength of 13.8 MPa per ASTM C476 (ASTM 2005e). The steel reinforcement was placed in every masonry block, creating a spacing of 0.41 m (1.33 ft) along the length of the retaining wall. The properties of the sound wall materials were based on the test data provided by the manufacturer, who also constructed the sound wall by an experienced and certified mason.

From the conducted tests (Fig. 2), the backfill soil used during the test consisted of sand with 2% gravel and 11% sand fines. The soil was classified as silty sand conforming to Caltrans grading system (Caltrans 1999). During the deposition of soil inside the container, nuclear gauge measurements of the compacted soil were taken at every 2 feet (lift height) of deposited soil to measure the unit weight and average moisture content of the compacted soil. The soil was compacted in a lift height of 610 mm (2 ft) using 27 kg gasoline-powered whackers to a 95% compaction requirement (Caltrans 1999). Based on the nuclear gauge measurements by certified lab technician at the site, the average unit weight (dry density) of the soil was 1824.5 kg/m$^3$ (113.9 lb/ft$^3$) for the first retaining wall test and 1818.1 kg/m$^3$ (113.5 lb/ft$^3$) for the second test. The average moisture content was verified to be 11.2% for both tests and the relative compaction was

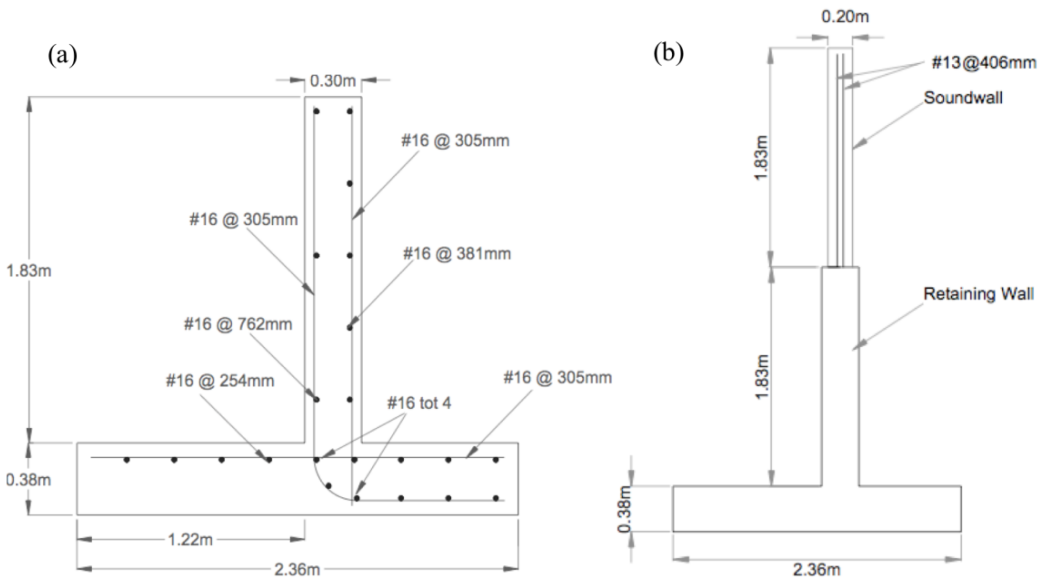


Fig. 1 Cross-section of retaining wall: (a) without sound wall; and (b) with sound wall

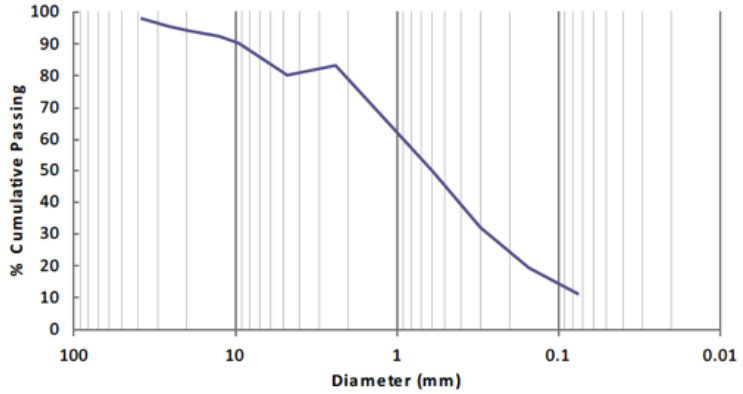


Fig. 2 Backfill soil grain size distribution range from conducted tests

Table 1 Backfill soil characteristics

| Property | Value |
|---|---|
| Gravel content (%) | 2 |
| Sand content (%) | 87 |
| Fines content (%) | 11 |
| Average moisture content (%) | 11.2 |
| Average dry density (kg/m$^3$) | 1821.3 |
| Friction angle (φ) (degree) | 48.7 |
| Soil cohesion (c) (kPa) | 0 |

95.3% and 95.0%, respectively. Monitoring sensors' reading changes during the compaction process was not feasible as it would not allow the completion of compaction within the scoped time frame of the project. Table 1 summarizes the main characteristics of this backfill soil based on sieve analysis test, triaxial test and direct shear test. Triaxial compression and direct shear tests were conducted in a certified soil lab on samples remolded as closely as possible to the field backfill placement conditions. Consolidated-undrained triaxial compression tests were performed (ASTM 2005f) by subjecting three separate specimens to respective cell pressures of 665, 718, and 744 kPa and then shearing to failure by increasing the deviator stress. The triaxial results suggested a total friction angle of 48.7° with zero cohesion intercept (0 kPa) and an effective friction angle of 40.8° with zero effective cohesion intercept (0 kPa). Direct shear tests were performed on new samples to failure at three different normal stresses. The results suggested a slightly smaller average friction angle of 38.4°.

### *2.3 Test configuration*

The retaining wall specimens were backfilled in a steel laminar soil container placed on the shake table. The laminar soil container was made of a series of W-shape steel ring sections with an inside dimension of 6.71 m (22 ft) long, 2.90 m (9.5 ft) wide and 3.35 m (11 ft) deep. The ring sections of the steel box were locked in place and restrained laterally to act as a rigid container. Two large steel towers were welded to the sides of the soil container via steel beams to provide additional lateral restraint. The soil box and towers were fixed to the shake table at the bottom,

such that the shake table induced unidirectional movement in the longitudinal direction. The retaining wall specimen was first positioned inside the soil container after a 1.07 m (3.5 ft) thick soil layer was deposited and compacted at the bottom of the container, as shown in Fig. 2(a). Once the wall was in position, additional 2.11 m (6.92 ft) thick soil layers were placed and compacted layer by layer inside the container. No soil was placed in front of the toe side of the footing and the sides of the wall were not constrained in the longitudinal direction, as shown in Fig. 3. These boundary conditions were selected to perform a conservative evaluation of wall performance without additional resistance provided by the toe side soil and the neighboring panels. This allows the wall to slide more, providing a more conservative design scenario. The backfill soil had a zero slope.

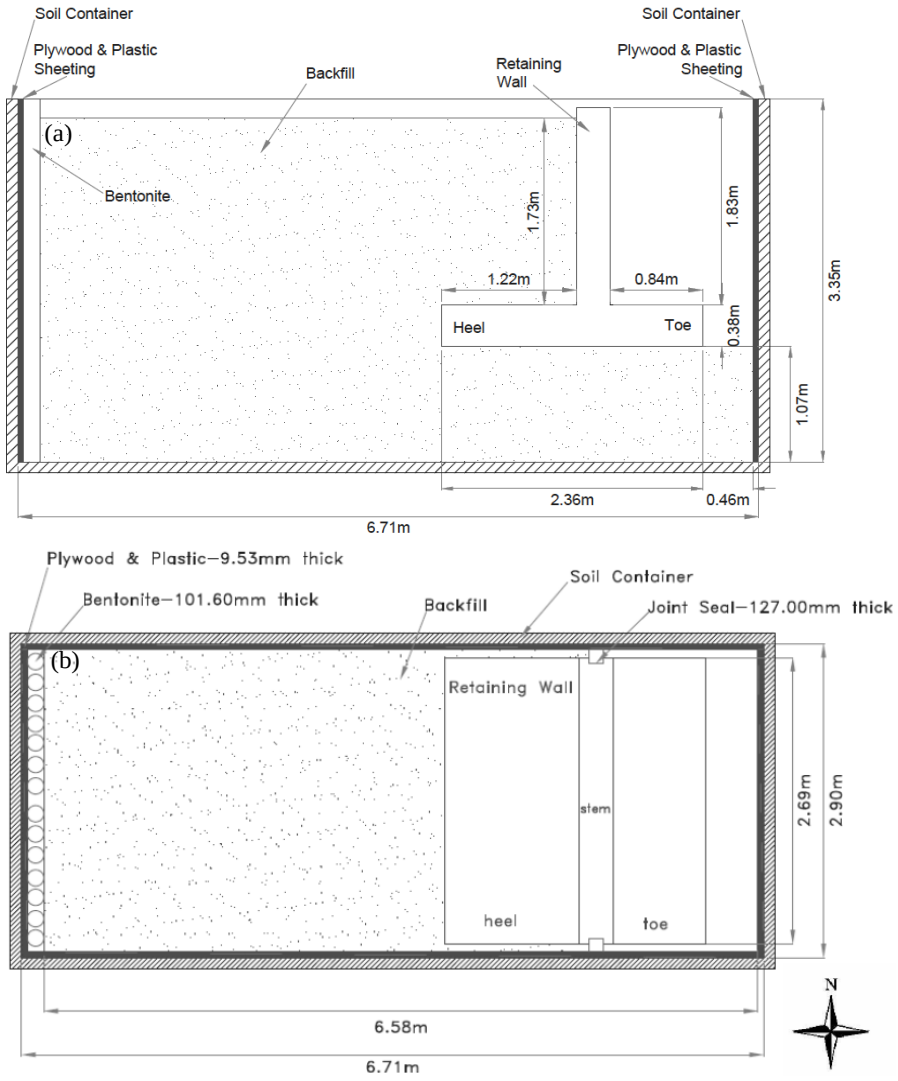


Fig. 3 Test configuration: (a) elevation view; and (b) plan view

To prevent any soil and water from leaking out of the steel box during the test, plywood was lined inside the soil container on all vertical sides and plastic sheeting was stapled onto the plywood, as shown in Fig. 3. The plastic sheeting was then greased to provide a frictionless boundary between the soil and the steel container. The frictionless boundary between the end surfaces of the wall and the steel container was ensured by inserting expansion joint seals that accommodate movement under compression, tension and shear, as shown in Fig. 3(b). Pockets were formed in both ends of the retaining wall in order to fit the joint seals. Furthermore, in order to minimize the reflection of the waves from the steel wall of the container back into the soil during the shakes, a 101.6 mm (4 in) thick layer of bentonite, a clay-like material, was placed on the far backside of the soil container (Fig. 3).

### *2.4 Input motions*

Three earthquake records were used as the input motions in the study: the 1994 Northridge (US-CA) earthquake, the 1999 Kocaeli (Turkey) earthquake, and the 1995 Kobe (Takatori, Japan) earthquake. The 1994 Northridge earthquake, as shown in Fig. 4(a), had a magnitude of 6.7 with the main shock lasting about 15 seconds. This earthquake is a high frequency shake and produced one of the strongest ground motions ever instrumentally recorded in an urban setting in North America, with extensive damages caused to structures (Mortezaei and Zahrai 2009). The Kocaeli earthquake of 1999, as shown in Fig. 4(b), is a relatively low frequency shake. It had a magnitude of 7.4 and a combination of low peak ground accelerations and long duration pulse (20 seconds).

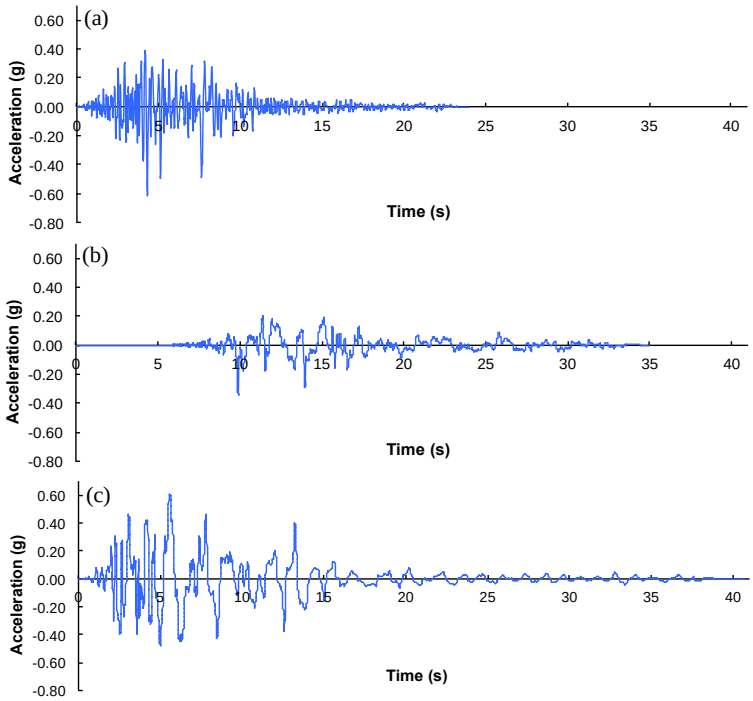


Fig. 4 Time histories of: (a) Northridge; (b) Kocaeli; and (c) Takatori earthquake

Table 2 Loading protocol with peak input values

| Scaling factor | Ground motion type | PGA (g) | PGV (m/s) | PGD (mm) |
|---|---|---|---|---|
| 0.25 | Northridge | 0.16 | 0.09 | 10.32 |
| | Kocaeli | 0.08 | 0.08 | 27.46 |
| | Takatori | 0.16 | 0.20 | 46.70 |
| 0.50 | Northridge | 0.32 | 0.18 | 20.64 |
| | Kocaeli | 0.15 | 0.17 | 54.92 |
| | Takatori | 0.31 | 0.40 | 92.88 |
| 0.75 | Northridge | 0.47 | 0.27 | 30.96 |
| | Kocaeli | 0.23 | 0.25 | 82.38 |
| | Takatori | 0.47 | 0.60 | 138.70 |
| 1.0 | Northridge | 0.63 | 0.36 | 41.29 |
| | Kocaeli | 0.31 | 0.34 | 109.84 |
| | Takatori | 0.62 | 0.80 | 185.77 |
| 1.5 | Northridge | 0.94 | 0.54 | 61.93 |
| 2.0 | Northridge | 1.26 | 0.71 | 82.57 |

This earthquake caused buildings to collapse, and was produced by a rapid and smooth bilateral fault rupture (Yagi and Kikuchi 2000). The 1995 Kobe earthquake (recorded from Takatori which is used as the designation of the earthquake motion throughout this paper) had a magnitude of 6.9 and duration of 7.5–12.5 seconds. This earthquake had a mixture of low and high frequencies, as seen in Fig. 4(c), and damaged half of the buildings (Mortezaei and Zahrai 2009). Additional data, such as response spectra of each earthquake, is available in PEER (2013).

### *2.5 Loading protocol*

All three earthquake records selected for the input motion (Northridge, Kocaeli, and Takatori) were performed at 25% intervals, increasing from 25% to 100% (corresponding to a scaling factor from 0.25 to 1.0) in each test scaled by the respective peak ground acceleration (PGA). The tests with the same respective scaling factor of ground motion were grouped together, as shown in Table 2. Additionally, the most representative earthquake motion in California (Northridge) was scaled to 1.5 and 2.0 (with a PGA of 0.94g and 1.26g, respectively) for final failure test, which were performed after the completion of all lower levels of the three earthquakes. The entire loading protocol is shown in Table 2, which also gives the peak ground acceleration (PGA), peak ground velocity (PGV) and peak ground displacement (PGD) for each ground motion. Prior to the beginning of each of the two tests, white noise shake at 3% root mean squared (RMS) for 5 minutes, and sine sweep input with a frequency change from 1 to 20 Hz and maximum amplitude of 0.075g, were applied to the shake table for initial characterization. For each test with and without sound wall, it should be noted that due to the use of same wall specimen throughout the loading sequence, dynamic responses to be discussed herein such as cracking, wall lateral displacement and backfill movement were cumulative, which would be different from individual test without any preexisting disturbance to the new wall-backfill specimen.

### *2.6 Instrumentation*

To acquire the dynamic response, the retaining wall-soil system was instrumented with accelerometers, microelectromechanical (MEM) based sensors (also known as soil inclinometers), linear variable displacement transducers (LVDTs), inclinometers, earth pressure cells, and strain gages (as illustrated in Fig. 5).

Signal conditioned accelerometers were placed inside the backfill soil and on the retaining wall to measure accelerations along the longitudinal and vertical direction in the soil and along the height of the stem. The accelerometers had dynamic ranges of ±2g to ±200g. As shown in Fig. 5, they were placed at three different depths inside the soil container. At each depth, there were 5 accelerometers (spaced at 0.76 m) in the longitudinal direction and 2 (spaced at 0.79 m) along the transverse direction. Along the stem of the retaining wall, 4 accelerometers were installed on the wall side with no backfill (2 on the very top of the stem and 2 in the mid-height of the stem). The MEM sensors used in this study are in-place inclinometer systems that were used to measure the relative horizontal and vertical displacements of the backfill soil before and after the shaking. Each sensor is made of a 3.2 m long tube encasing a series of 10 equally spaced inclinometers long the length. Two rows of MEM sensors with 5 in each (spaced at 0.79 m) were placed in the backfill soil, as shown in Fig. 5, resulting in 10 units in total. Each unit was fixed to the bottom of the steel container via a specially designed socket type base support. All the sensors were then connected to a network controller module that communicates the measurements to a server through a wireless modem. To measure the vertical displacement (heave or settlement) in the

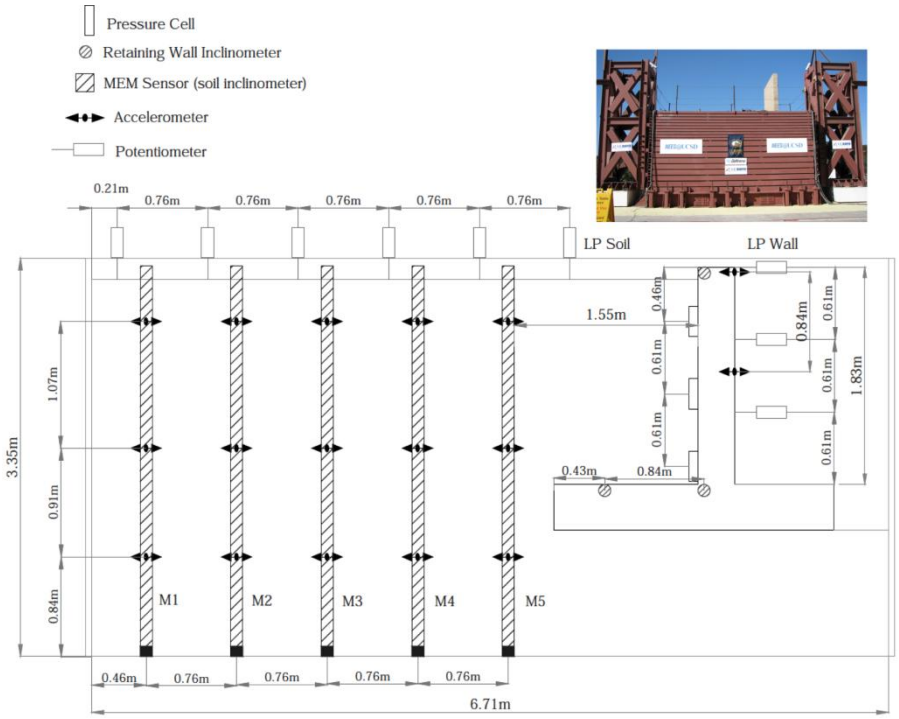


Fig. 5 Elevation view of soil container with instrumentation layout

backfill soil, 12 LVDTs were installed in two rows on the top surface of the backfill (the set labeled by "LP Soil" in Fig. 5). The LVDTs were spaced 0.76 m apart along the longitudinal direction and 0.91 m apart along the transverse direction. An aluminum frame was fabricated and bolted to the top of the steel container to hold the LVDTs upright. To allow for free sliding of the LVDTs in the longitudinal direction during shaking, thin smooth laminated boards were also placed underneath the tip of the LVDTs.

To measure the lateral movements of the wall, 9 linear potentiometers (the set labeled by "LP Wall" in Fig. 5) were placed on the backside of the wall, spaced at an interval of 0.61 m along the height of the stem and 0.66 m along the transverse direction, i.e., in a 3 by 3 array. Capacitance-based inclinometers (rotational device) were mounted at 6 locations on the retaining wall (stem and footing) using aluminum plates and bolts to monitor the bending, inclination, and rotation of the wall during the shaking. The inclinometers have a total range of ±60 degrees and a linear range of ±45 degrees.

To directly measure the dynamic lateral earth pressure behind the retaining wall, a series of earth pressure cells with a range of 0~200 kPa were mounted on the wall along the height of the stem (on the side in contact with the backfill soil). In the test without sound wall, the pressure cells were installed at three different heights along the stem (with a spacing of 0.61 m), as depicted in Fig. 6(a), while they were installed at four different heights in the second test with wound wall (spaced 0.30 m apart), as shown in Fig. 6(b). Originally there were 2 cells installed 0.61 m apart at each height, but a couple of them malfunctioned during the test and therefore, were removed from Fig. 6. Square mounting steel plates were prefabricated to host the pressure cell unit where the plates had an indented circle in the middle. Quick-setting mortar was placed between the mounting steel plates and the concrete wall surface to ensure a smooth contact (Bentler and Labuz 2006).

To monitor the structural damage in the retaining wall, lead-attached strain gages were installed on the reinforcing steel bars inside the concrete wall. They were placed along the wall height (spaced at 0.38 m apart) on every other transverse rebar (see Fig. 1). A grid pattern consisting of 0.30 by 0.30 m grids was created on top of the compacted backfill soil in order to track the potential cracks in the soil. White sand was used to create such a grid in the first test, and was replaced with orange spray paint during the second test for a better visibility.

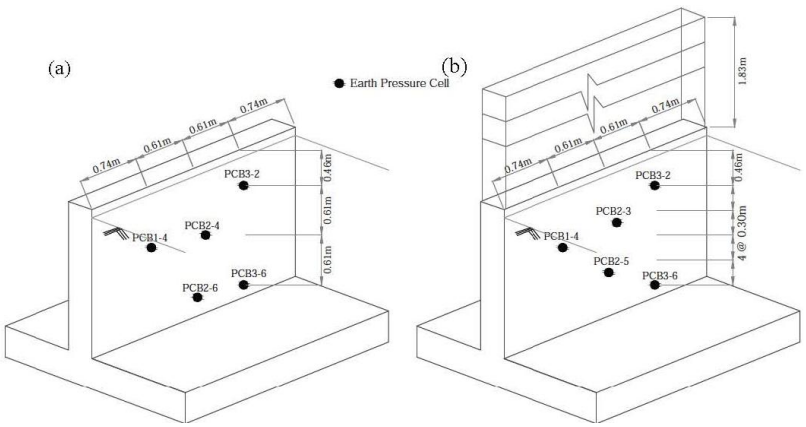


Fig. 6 Location of earth pressure cells for test: (a) without sound wall; and (b) with sound wall

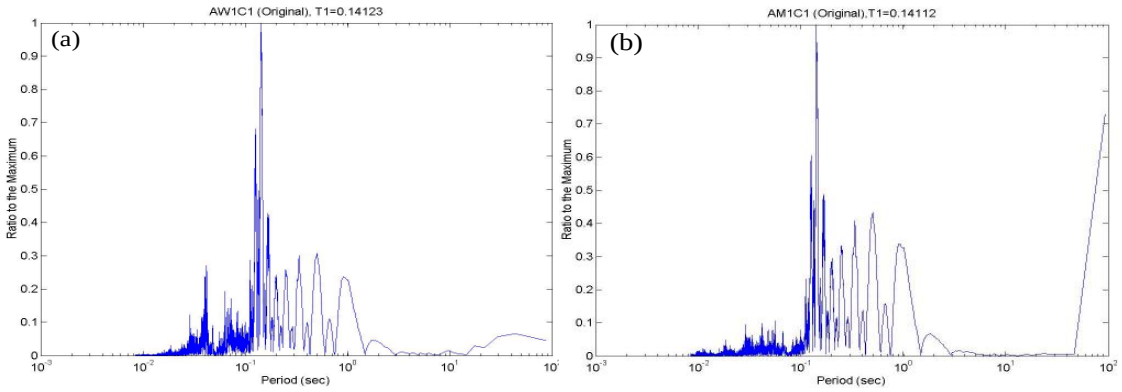


Fig. 7 Initial characterization under sine sweep input using FFT: (a) AW1C1 (wall acceleration); and (b) AM1C1 (backfill acceleration)

## 3. Test results for retaining wall without sound wall

### *3.1 Initial characterization under sine sweep*

Small sine sweep input was applied to the table prior to the test for initial characterization. The sine sweep had a frequency change from 1 Hz to 20 Hz and maximum amplitude of 0.075g. A standard Fast Fourier Transform (FFT) method was used to investigate the frequency content of the accelerations measured from 4 accelerometers installed on the wall (AW1C1 – AW2C2) and 30 installed inside the backfill (AM1C1 – AM10C3). Fig. 7 shows the typical FFT analysis results of the wall accelerations (AW1C1 on the left) and the backfill accelerations (AM1C1 on the right). The accelerations on the vertical axis were normalized by the maximum that occurred at the fundamental period (i.e., ratio to the maximum). It can be seen that the fundamental period of the soil-wall system was about 0.141 seconds and the corresponding frequency is $\omega = 44.56$ rad/sec.

### *3.2 Backfill behavior*

A crack in the backfill soil first started to develop during the Takatori 0.75 motion. This crack occurred in the soil at the top surface approximately 1.35 m from the heel side of the footing, which was about 2.57 m measured from the edge of the stem of the retaining wall (as shown in Fig. 8). The inclination of this active soil failure plane ($\alpha$), measured from the horizontal direction, typically defines the direction of the failure plane, which is the bottom plane of the critical soil wedge mobilized at active failure condition (Koseki et al. 1998). Assuming a linear representation, this first active failure plane connecting the corner of the heel to the location of this failure crack on the top soil surface would yield a failure plane angle ($\alpha$) of 57.4° (measured counterclockwise from the horizontal bottom edge of the footing). This failure plane angle is 12.9% more than the predicted angle using the conventional Mononobe-Okabe method (US Army Corps of Engineers 2012), where the failure plane angle is calculated as 50° using the measured total soil friction angle in Table 1 and assuming the soil-wall friction angle to be zero. During the subsequent shakes, more cracks were developed having larger width, with the exception of the Kocaeli shakes. More cracks were observed at locations closer to the retaining wall than anywhere

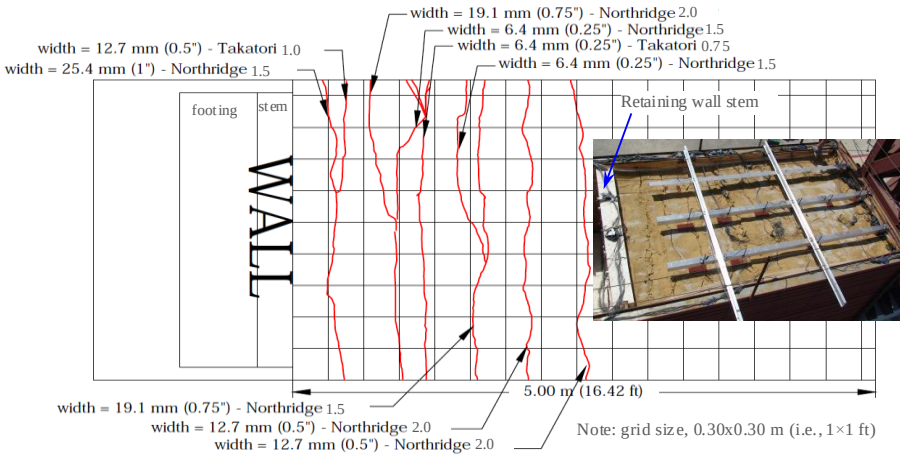


Fig. 8 Crack pattern in backfill for retaining wall without sound wall

else along the longitudinal direction (shaking direction). Some of these cracks gradually propagated in the transverse and vertical directions. During the Northridge 1.5 and 2.0 tests, the cracks near the back of the retaining wall further formed a dominant slip plane that created a gap between the stem and the compacted soil, where an apparent thrusting action was observed. This thrusting action was due to the out of phase movement of the wall and soil mass during the last two shakes. A possible interpretation for such a large soil mass would be that, because of suction due to partial saturation of the soil (i.e., 11% moisture content), there was a substantial depth that, at least under small accelerations, does not require support; and therefore gaps and out of phase movements develop during shakes at higher intensity. Fig. 8 shows the crack pattern development in the backfill soil with the crack size measured at the end of the test.

During the shakes, the amount of dynamic lateral displacement response of the backfill measured by the accelerometers increased along the depth of the soil (zero depth is defined at the bottom). The permanent horizontal movement of the backfill soil along the depth of the soil (zero at the bottom) is shown in Fig. 9, based on the results of the MEM sensors relative to the fixed base measured before and after each shake. The location of the sensors is indicated on top of each plot by the distance measured from the stem of the wall (M5 is the closest and M1 is the farthest to the wall). It can be seen that the horizontal displacement of the soil has a nonlinear increasing trend along the depth of the soil. It also increased as the intensity of the shake was increased (from Takatori 1.0 to Northridge 1.5). During the Northridge 1.5 shake, the soil in the backfill was significantly more disrupted and loosened compared with the previous shakes with the largest horizontal displacement measured as 13.04 mm at the top. This relative displacement increased to 44 mm at the end of the Northridge 2.0 shake. The trend of this horizontal movement of the backfill soil along the depth was also confirmed by the acceleration measurements where the accelerometers were embedded at three depths of the backfill (Fig. 6). It can also be seen from Fig. 9 that at the end of the Northridge 1.0 shake, the soil crack on the top surface near the back of the retaining wall propagated about 0.30 m down into the backfill, as indicated by the sudden change of the slope of the response curve for M5, M4 and M3 in Fig. 9 (where M5 was the closest to the retaining wall). This crack propagation along the depth was less obvious for locations farther away from the back of the wall, e.g., M2 and M1 that were 3.88 m and 4.64 m away from the stem,

respectively. During subsequent shakes, cracks continued to propagate gradually into the backfill soil, and by the end of the Northridge 1.5 test, the propagation reached an approximate depth of 2.26 m from the top surface (i.e., 0.91 m from the bottom of the MEM sensors, as indicated by the sudden slope change in the curve in Fig. 9).

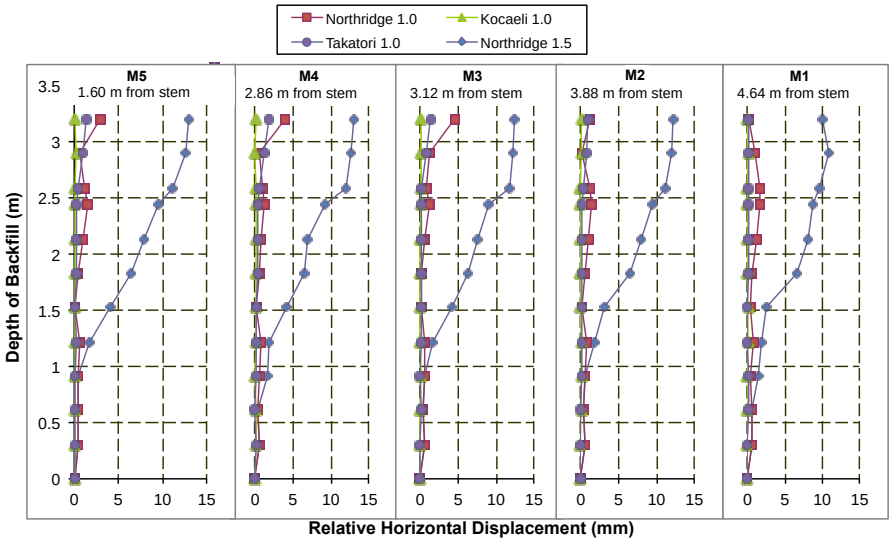


Fig. 9 Relative horizontal displacements from MEM sensors in the backfill in test without sound wall

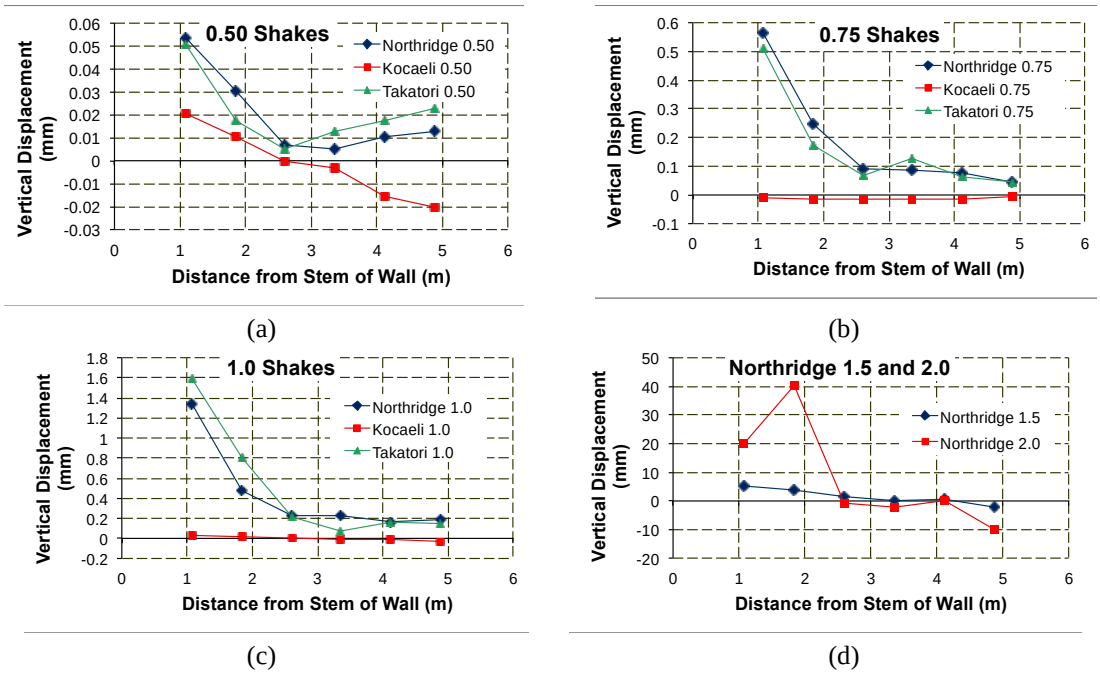


Fig. 10 Peak vertical displacements of backfill in test without sound wall during: (a) 0.50 shakes; (b) 0.75 shakes; (c) 1.0 shakes; and (d) Northridge 1.5 and 2.0 shakes

For the vertical movement of the backfill soil (i.e., settlement or heaving), little response was observed prior to the 0.75 shakes in the soil. As the intensity of the ground motions increased, a considerable amount of vertical displacement was observed in the soil near the back of the retaining wall. Fig. 10 shows the peak vertical displacements on the backfill surface along the longitudinal direction of the box during each of the shakes (note that the horizontal axis represents the distance of the backfill soil measured from the stem of the retaining wall). It can be seen that, in general, the largest vertical displacement occurred near the back of the retaining wall, and the displacement decreased as it moved towards the far end of the soil container. Most of the displacements showed positive values in the vertical axis, implying upward movements of the soil (i.e., heaving rather than settling type of motion). This can be explained by the fact that soil cracks started to form and propagate near the back of the wall stem during those shakes. When the compacted soil moved back toward the wall during shaking, the soil started to build up, which created heaving close to the wall. Among all the ground motions, the Kocaeli shakes had minimal effect on the vertical response of the backfill soil (even with the 0.5 shake since the magnitude was very small). Settlement was observed near the far end of the soil container during the Northridge 1.5 and 2.0 tests. During the Northridge 2.0 test, the vertical displacement had a sudden increase at a distance of 1.84 m from the wall stem. This was mainly caused by the thrusting action of the compacted soil mass after the major crack opened up forming the dominant slip plane in the backfill near the stem of the wall, as previously discussed.

### *3.3 Wall lateral displacement*

### *3.4 Lateral earth pressure along the height of stem*

Fig. 12 shows the progression of the peak dynamic lateral pressure along the height of the stem from the 0.25 to the 1.0 Northridge motions. Note that the initial static pressure before the test was subtracted from the total pressure at the peak acceleration of the shake to obtain the peak dynamic pressure discussed herein. The peak pressure measurements in the figure were taken at the peak acceleration of the Northridge, Kocaeli, and Takatori earthquakes. In general, the earth pressure cells installed near the middle of the stem (0.76 m from the bottom of the stem) measured the greatest dynamic response (with the greatest of 12.1 kPa measured in the Northridge 1.0 shake). The lateral pressure also increased as the intensity of the earthquake motion increased, where this increase is more substantial near the bottom than near the top of the stem. Moreover, it can be seen from Fig. 12 that the distribution of the peak pressure along the height of the stem exhibits a nonlinear trend with the maximum towards the mid-height. A similar trend was also observed during both the Kocaeli and Takatori motions (not shown in the figure). Among the three earthquakes with the same respective intensity (i.e., 0.25, 0.50, etc.), the lateral pressure was measured to be the smallest in Kocaeli and generally the greatest in Takatori for most of the shakes except for the mid-height location in the 1.0 shake (where Northridge 1.0 generated the highest pressure).

This nonlinear trend of active earth pressure distribution has also been discussed in several other studies in the literature (Fang and Ishibashi 1986, Paik and Salgado 2003, Jung and Bobet, 2008). According to Paik and Salgado (2003), a so-called “arching effect” exists and could be the major cause of this nonlinear pressure distribution. The arching effect is typically developed in the soil when the retaining wall moves away from the backfill and a soil wedge slides down behind

the wall. This causes the stress to redistribute and transfer around the local region of the soil, which reduces the local stress in the soil with a reduction in the pressure cell measurement. It is also pointed out by Fang and Ishibashi (1986) that translation wall movement, which is the primary mode observed in this test, could cause the distribution of the active horizontal pressure to be roughly parabolic. This nonlinear trend of the dynamic pressure distribution observed during the test was also comparable to what was observed in a recent study using a similar shake-table test setup (Wilson and Elgamal 2009), where a 1.7 m (5.5 ft) high bridge abutment wall backfilled with soil was tested to record the passive force-displacement as well as the dynamic earth pressure under scaled earthquake motions.

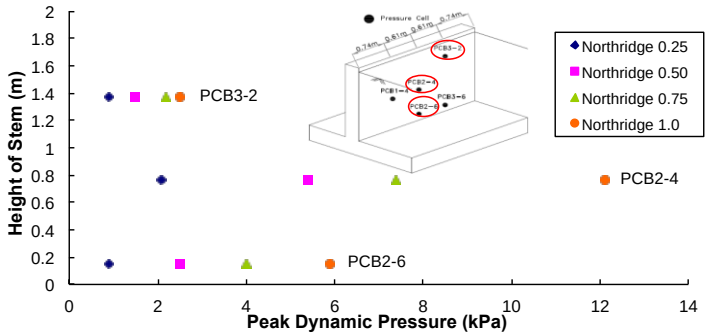


Fig. 12 Peak dynamic pressure along the height of the stem measured by earth pressure cells for Northridge shakes in test without sound wall

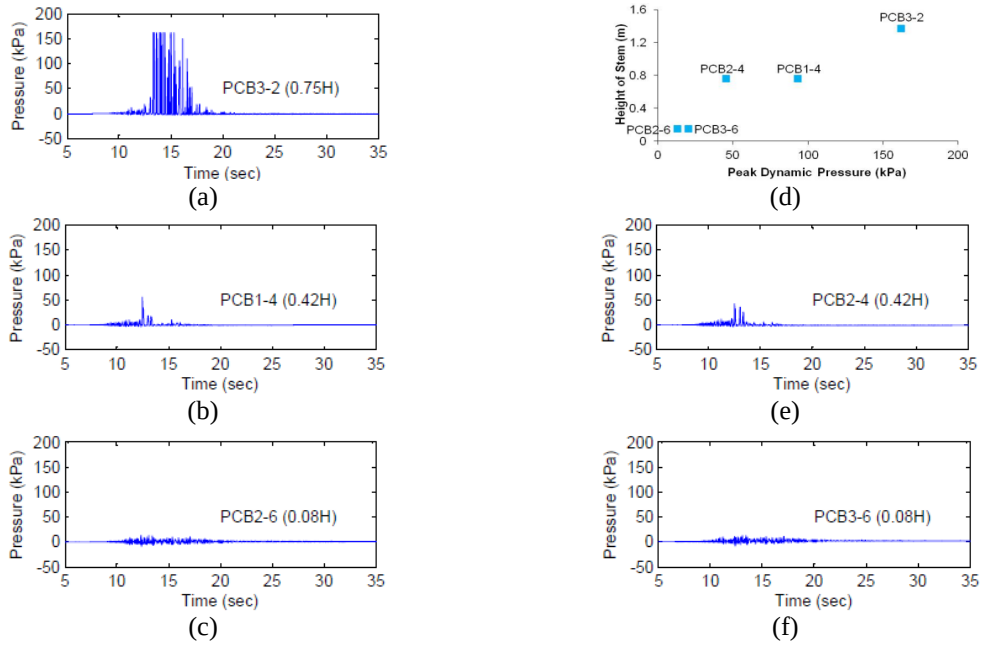


Fig. 13 Dynamic response of pressure along the height of the stem in Northridge 2.0 in test without sound wall measured by earth pressure cells: (a) PCB3-2; (b) PCB1-4; (c) PCB2-4; (d) PCB2-6; (e) PCB3-6; and (f) peak pressure in all cells

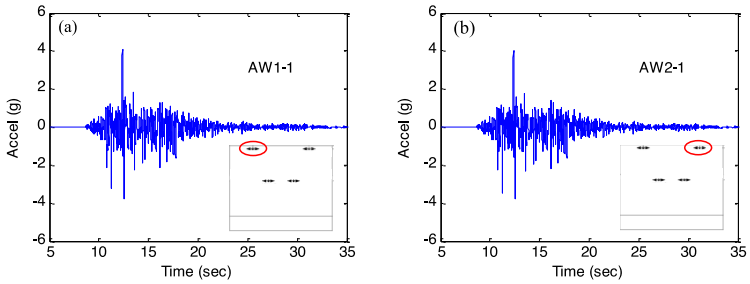


Fig. 14 Time history response of wall acceleration at the top during Northridge 2.0 in test without sound wall: (a) AW1-1 (south end); and (b) AW2-1 (north end)

During the Northridge 1.5 test, the distribution of the lateral pressure followed a similar nonlinear trend to the previous shakes. It then changed to a different pattern during the 2.0 shake. Figs. 13(a), (b), (c), (d) and (e) illustrate the Northridge 2.0 time history of the dynamic pressure in cells PCB3-2, PCB1-4, PCB2-4, PCB2-6 and PCB3-6 respectively. Fig. 13(f) gives the dynamic pressure at the peak acceleration from each of these cells along the stem height. It can be seen that the pressure cell near the top of the stem (PCB3-2) started to measure more dynamic response than the middle ones (PCB1-4 and PCB2-4), differing from previous shakes, and that this pressure reached a maximum level of 162 kPa at the peak acceleration near the top, as shown in Fig. 13(a). This change of pressure distribution was mainly due to the fact that a large gap already formed at the upper part of the stem between the wall and the soil directly behind the wall before the last shake. Under the high intense shake of Northridge 2.0, the soil mass was driven into the wall creating higher dynamic pressure thrusts than the middle and the bottom. This was also confirmed by the time history response of the wall horizontal acceleration. The accelerometers placed at the top of the retaining wall measured the largest response at the peak of the Northridge 2.0 shake, as shown in Fig. 14 (AW1-1 on the south end and AW2-1 on the north end, both at the top of the wall), indicating the largest lateral wall movement into the backfill near the top.

In addition to the direct means of pressure measurement via pressure cells, the strain data measured by the strain gages installed on the steel rebars along the wall stem was also examined to qualitatively estimate the lateral pressure behind the wall. Bending moments were first back calculated from the strain measurements along the wall, and the lateral pressure was then obtained by differentiating the bending moment following the Euler–Bernoulli Beam Theory (Gere and Timoshenko 1997). The peak dynamic pressure thus estimated is shown in Fig. 15 for all cases. Note that the strain gages located near the top of the stem recorded sufficient noise such that the dynamic pressure at the peak acceleration could not be extracted from their dynamic response. Nevertheless, it can be seen that the pressure distribution based on the strain gage measurements displayed a quite linear trend along the depth of the stem. During the Northridge 1.5 and 2.0 tests, a much larger amount of pressure was measured near the bottom of the stem than the previous shakes, and the pressure distribution changed drastically from the linear trend. Fig. 15 also compares the peak dynamic pressure obtained from the strain gage measurements to the pressure cell readings as previously discussed. It is quite obvious that they provided different pressure distribution profiles along the depth of the wall (i.e., a linear trend vs. a nonlinear shape). The pressure distribution indirectly measured by the strain gage readings was not affected by the local arching effect near the bottom of the stem as experienced in the pressure cells that were in direct

contact with the soil.

It is worthy of note that the static pressure prior to dynamic testing was found to be the greatest about half way up the stem (0.42H, where H is the total height of the stem) and close to zero near the bottom of the stem (0.08H). Similar observation was reported in an existing literature (Wilson 2009), where the reduction in pressure near the bottom was explained by a very slight movement of the test wall away from the backfill near the bottom that affected the contacting area between the soil and the pressure cell. This static pressure distribution is not in good agreement with the well-known classical Rankine theory for a rigid and unyielding wall. Theoretically, this static pressure is estimated to vary linearly along the height of the wall stem, from zero at the top of the wall and a maximum at the bottom of the stem. One possible cause of this different static pressure

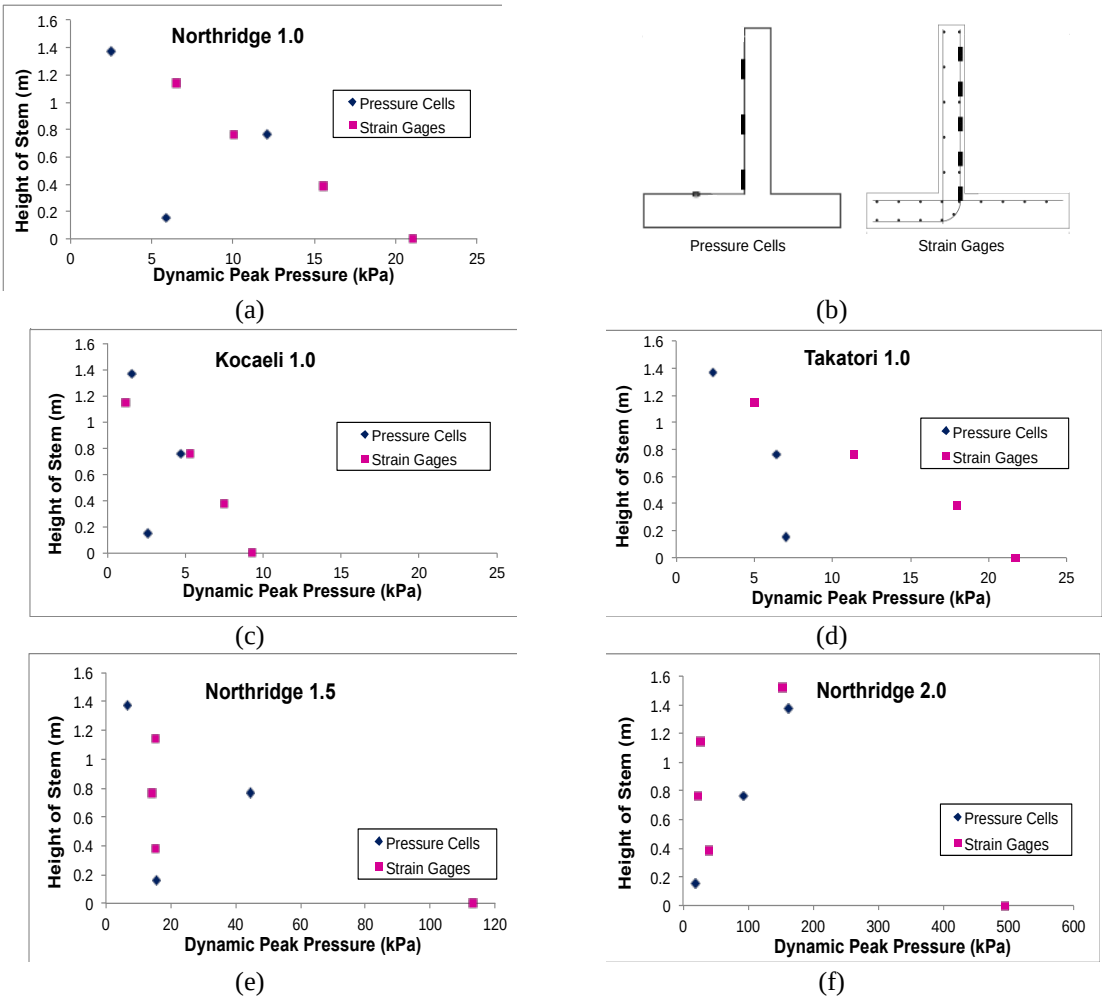


Fig. 15 Comparison of peak dynamic pressure based on pressure cell and strain gage in test without sound wall: (a) Northridge 1.0; (b) locations of measurements; (c) Kocaeli 1.0; (d) Takatori 1.0; (e) Northridge 1.5; and (f) Northridge 2.0

distribution can be attributed to the compaction of soil behind the wall during the construction stage, as further addressed by Bentler and Labuz (2006), as well as Aggour and Brown (1974). Their efforts show that compaction can cause the static pressure along the height of the wall to differ from the pressure distribution predicted by conventional static earth pressure theories. Aggour and Brown (1974) also performed numerical simulations to study the effect of compaction on lateral pressures along the height of the retaining wall. It is stated in their paper that when loose sand is compacted, the density of the sand is increased, thus increasing its stiffness. The major factors that could affect the static pressure are the number of compacting passes, the end wall constraints, the flexibility of the wall, and the backfill geometry.

## 4. Comparison of tests with and without sound wall

### *4.1 Backfill behavior*

During the test with sound wall, the first soil crack occurred in the backfill during the Northridge 1.0, slightly later than the test without sound wall where the first failure plane occurred during the Takatori 0.75. This first soil crack was developed approximately 0.53 m from the edge of the footing heel, which was about 1.75 m from the edge of the stem. Compared to the previous test, this crack occurred much closer to the backside of the retaining wall. If following the same linear assumption for failure plane, the failure plane angle in this test was 75.8°, which is 32% greater than the test without sound wall. No crack formed in the soil during the Kocaeli and

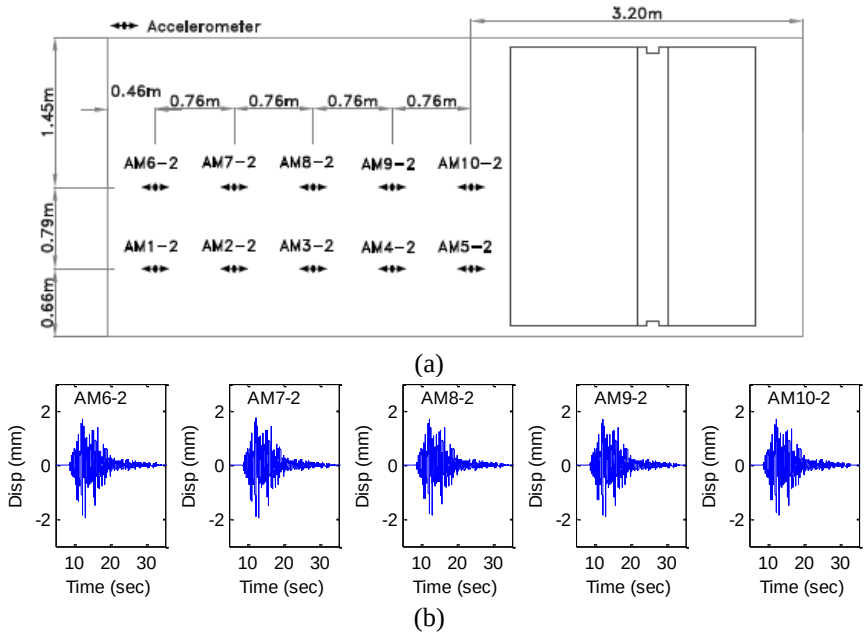


Fig. 16 Comparison of dynamic horizontal displacement response of backfill at north side during Northridge 1.0 motion: (a) locations of accelerometers in the backfill; (b) test without sound wall; and (c) test with sound wall

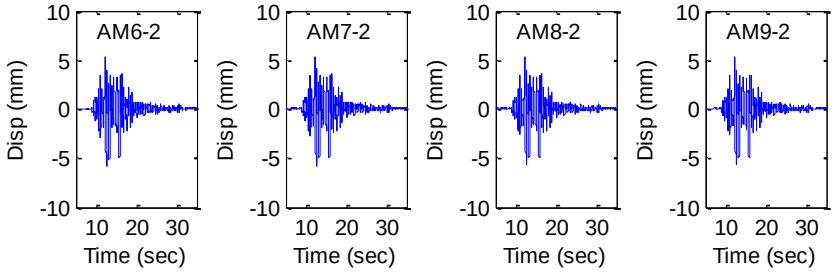


(c)
Fig. 16 Continued

Takatori shakes. Similar to the test without sound wall, most soil damage occurred during the last two shakes (i.e., Northridge 1.5 and 2.0) with several exterior slip planes (soil cracks) developed in the backfill. The cracks propagated to a depth in the soil similar to the previous test. The profile of the horizontal movement before and after each shake of the backfill soil along the length of the container and the depth of the wall was also found to be similar to the test without sound wall based on results from the MEM sensor measurements. However, during the shakes with higher intensity, the backfill soil behind the wall with sound wall experienced more dynamic horizontal displacement response than the backfill in the previous test. Fig. 16 illustrates such a comparison for the Northridge 1.0 shake based on the accelerometers embedded in the backfill in the mid-height level (1.77 m from the bottom of the soil container). For the vertical displacement of thesoil, the LVDTs installed on the top of the soil generally measured more displacement during this test than the previous one without sound wall. However, the overall response trend was similar, where heaving type of motion was observed more than settlement at the soil surface.

### *4.2 Wall lateral displacement*

Compared to the previous test, the retaining wall with sound wall had similar relative horizontal displacements during the lower shakes (i.e., 0.25, 0.50 and 0.75), as shown in Fig. 17(a) based on the string potentiometer measurements. The solid lines with filled markers represent the results from the first test without sound wall, while the dotted lines with unfilled markers are for the second test with sound wall. During the 1.0 shakes, these relative horizontal displacements were found to be smaller in the test with sound wall than the one without [Fig. 17(b)], except for the Kocaeli shake. This is mainly due to the increased weight from the masonry sound wall in the second test. However, during the subsequent shakes, the higher excitations of Northridge 1.5 and 2.0 generated much more lateral movements in the retaining wall with sound wall than the previous one without sound wall, i.e., 12% and 16% more for Northridge 1.5 and 2.0, respectively, as seen in Fig. 17(c). The post-test inspection of the wall structure also revealed that the retaining wall with sound wall experienced much more cracking in concrete at the joint of stem and footing, as compared to the previous test without sound wall. Cracking in the mortar joints of the masonry blocks and at the masonry-to-concrete interface was also noticed starting from the 0.75 Northridge shake. Although the sound wall was excited to experience high accelerations (up to 7g) and large swinging motions during the intense shakes, it remained intact and no collapse occurred.

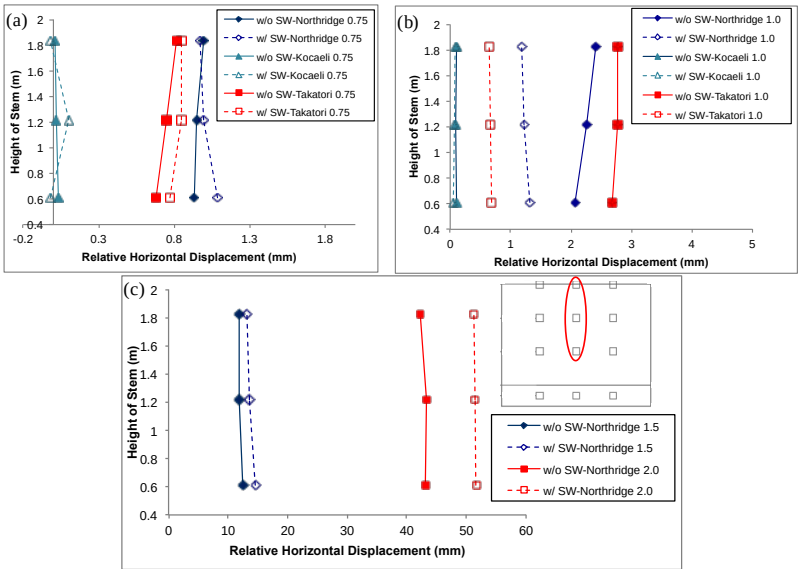


Fig. 17 Comparison of relative horizontal displacement measured by string potentiometers for tests with and without sound wall during: (a) 0.75 shakes; (b) 1.0 shakes; and (c) 1.5 and 2.0 hakes

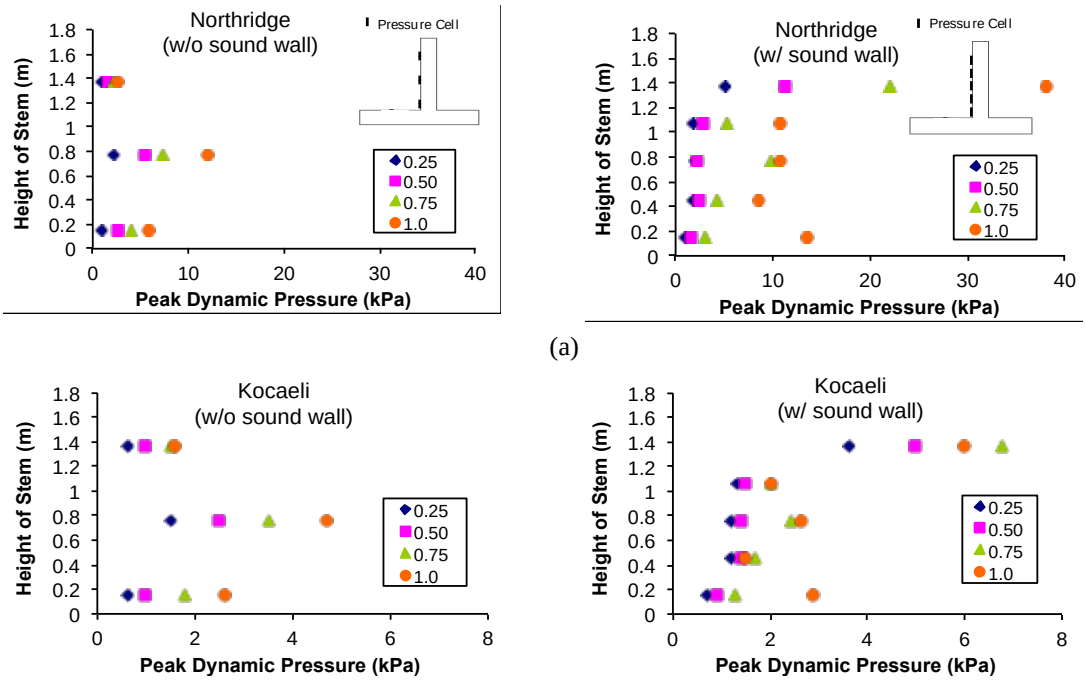


Fig. 18 Comparison of peak dynamic pressure along height of the stem for test with and without sound wall under: (a) Northridge; (b) Kocaeli; (c) Takatori; and (d) Northridge 1.5 and 2.0 motions

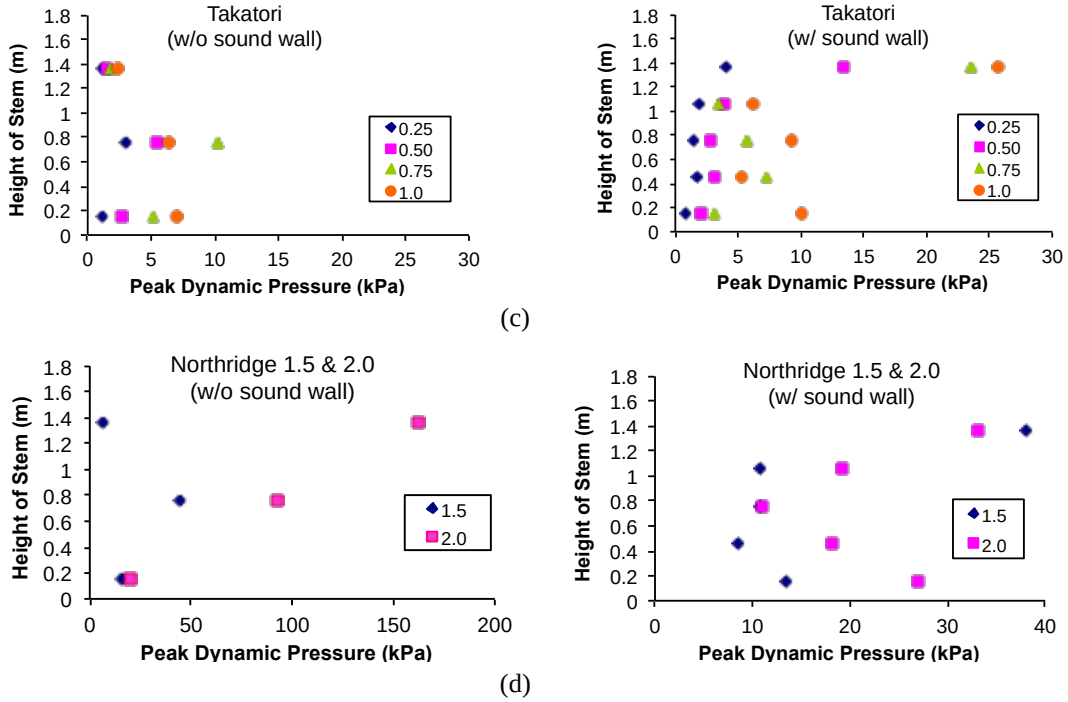


Fig. 18 Comparison of peak dynamic pressure along height of the stem for test with and without sound wall under: (a) Northridge; (b) Kocaeli; (c) Takatori; and (d) Northridge 1.5 and 2.0 motions

### *4.3 Lateral earth pressure along the height of stem*

Fig. 18 compares the peak dynamic pressure along the height of the stem measured by earth pressure cells in both tests. Compared to the previous test without sound wall, the earth pressure on the retaining wall with sound wall displayed more nonlinearity (polynomial shape) along the height of the stem, as shown in plots on the right-hand side of Fig. 18. Moreover, the largest dynamic pressures were measured near the top of the stem, rather than the middle as seen in the previous test. This was likely caused by the reverse thrust of the stem towards the soil near the top due to the existence of the large sound wall mass on top of the retaining wall. As the sound wall was excited during the shakes, the large inertia of the structure drove the wall to move out of phase with and towards the top layer of the soil, introducing the reverse thrusting effect into the stem. This reverse thrusting effect produced significant pressure near the top and also caused the failure plane to occur closer to the back of the retaining wall, as compared to the previous test without sound wall.

During the less intense shakes (i.e., 0.25, 0.50 and 0.75), the measured peak dynamic pressure at the bottom and mid-height of the stem with sound wall was generally more than the pressure behind the wall without sound wall at similar heights. In the test with sound wall, the peak pressure near the bottom of the stem (measured by PCB3-6) showed the smallest value along the height from 0.25 to 0.75 shakes under all three earthquake motions. After the 0.75 shake, this

pressure rapidly increased and exceeded the pressure level at the mid-height. This was not observed during the previous test without sound wall (as seen in the plots on the left-hand side of Fig. 18), where the pressure cells near the bottom of the stem always measured the smallest amount of peak pressure. This difference could be due to the large increase of the flexural flexibility of the wall with sound wall during more intense shakes, where the wall experienced much more cracking at the stem-footing joint (during the 1.0 and above shakes) than the previous wall without sound wall. According to the results from a numerical study in the literature, the flexural flexibility of a retaining wall has been found to affect the seismic earth pressure behind the wall in addition to the horizontal translation of the wall (Jung and Bobet 2008).

It is noted that during the Northridge 2.0, the lateral pressure near the top of the stem in the test without sound peaked at 162 kPa, while this pressure was only about 33 kPa in the test with sound wall, as shown in Fig. 18(d). As explained previously, this was mainly due to the fact that in the test without sound wall, a large gap formed in the soil next to the wall stem during the Northridge 2.0 test, where the soil mass was driven into the wall creating higher dynamic pressure.

## 5. Assessment using Mononobe-Okabe method

To evaluate the earth pressure behind the retaining wall, the existing Mononobe-Okabe method is adopted. The total friction angle (φ) measured from the triaxial test (Table 1) and the soil unit weight ($\Upsilon_s$) verified by the nuclear gage test were used. The soil-wall friction angle (δ), the slope of back of the wall (β), and the backfill slope angle (*i*) were assumed to be zero. The accelerations that were used to evaluate the M-O soil pressures were the peak accelerations taken from Table 2, e.g., 0.63g for Northridge 1.0 earthquake motion. The comparison on resultants and their locations

Table 3 Comparison of resultants and locations of dynamic earth pressure

| Input motion | Pressure cell results | | | | Analysis using M-O method | | Percent difference* | | | |
|---|---|---|---|---|---|---|---|---|---|---|
| | Test without SW | | Test with SW | | | | Test without SW | | Test with SW | |
| | Resultant (kN/m) | Location (×H‡) | Resultant (kN/m) | Location (×H‡) | Resultant (kN/m) | Location (×H‡) | R (%) | H (%) | R (%) | H (%) |
| Northridge 0.25 | 2.29 | 0.48 | 4.59 | 0.65 | 2.08 | 0.33 | 9.2 | 31.3 | 54.7 | 49.2 |
| Kocaeli 0.25 | 1.59 | 0.48 | 3.20 | 0.66 | 0.97 | 0.33 | 39.0 | 31.3 | 69.7 | 50.0 |
| Takatori 0.25 | 3.06 | 0.48 | 3.87 | 0.64 | 2.08 | 0.33 | 32.0 | 31.3 | 46.3 | 48.4 |
| Northridge 0.50 | 5.43 | 0.45 | 8.42 | 0.70 | 4.81 | 0.33 | 11.4 | 26.7 | 42.9 | 52.9 |
| Kocaeli 0.50 | 2.64 | 0.48 | 4.13 | 0.67 | 1.93 | 0.33 | 26.9 | 31.3 | 53.3 | 50.7 |
| Takatori 0.50 | 5.45 | 0.43 | 10.48 | 0.69 | 4.61 | 0.33 | 15.4 | 23.3 | 56.0 | 52.2 |
| Northridge 0.75 | 7.80 | 0.44 | 18.06 | 0.68 | 8.13 | 0.33 | -4.2 | 25.0 | 55.0 | 51.5 |
| Kocaeli 0.75 | 3.95 | 0.47 | 5.72 | 0.67 | 3.18 | 0.33 | 19.5 | 29.8 | 44.4 | 50.7 |
| Takatori 0.75 | 9.68 | 0.41 | 18.01 | 0.69 | 8.13 | 0.33 | 16.0 | 19.5 | 54.9 | 52.2 |
| Northridge 1.0 | 11.73 | 0.42 | 32.69 | 0.65 | 12.80 | 0.33 | -9.1 | 21.4 | 60.8 | 49.2 |
| Kocaeli 1.0 | 5.11 | 0.45 | 5.81 | 0.61 | 4.61 | 0.33 | 9.8 | 26.7 | 20.7 | 45.9 |
| Takatori 1.0 | 8.69 | 0.39 | 22.48 | 0.64 | 12.64 | 0.33 | -45.5 | 15.4 | 43.8 | 48.4 |

*Percent difference = (Test – Analysis)/Test×100%;

‡H = height of the stem filled with backfill soil measured from the bottom of stem

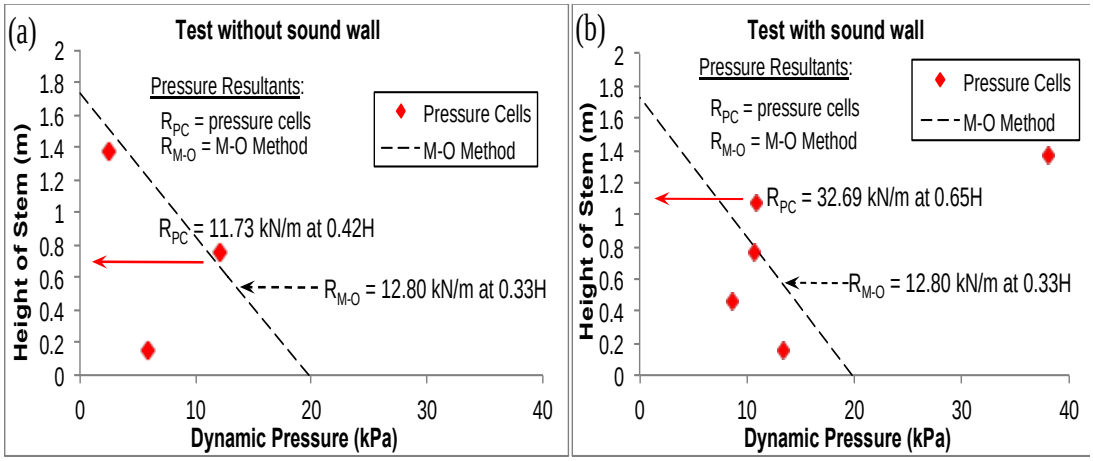


Fig. 19 Comparison of Mononobe-Okabe method to measured lateral dynamic pressure under Northridge 1.0 for: (a) test without sound wall; and (b) test with sound wall

for all earthquake input motions is shown in Table 3 with the percent difference with respect to the test results summarized as well. Due to the limitations of the M-O method when high peak ground accelerations are used, the Northridge 1.5 and 2.0 cases are excluded from this comparison.

Fig. 19 further illustrates such a comparison for the Northridge 1.0 shake in both tests as an example. The resultants of the peak lateral dynamic earth pressure directly measured by the pressure cells were calculated using tributary area. In both plots, $R_{M-O}$ is according to the M-O method and $R_{PC}$ is based on the measured data during the test. It can be seen that the linear pressure distribution using the M-O method is different from the nonlinear pressure measured from the test. The M-O method estimated the resultant of the pressure to be 12.80 kN/m, acting at a height of 0.33H (i.e., one-third the backfill height measured from the bottom of the stem, where H is the backfill height). For the test without sound wall as shown in Fig. 19(a), this estimation was about 9.1% more than the measured dynamic pressure resultant and the location of the resultant was lower than the test result (i.e., 0.42H instead of 0.33H). This difference is significantly more for Kocaeli and Takatori input motions, as summarized in Table 3. For the test with sound wall [Fig. 19(b)], the M-O method largely underestimated both the pressure resultant and the height of the resultant. This also applies to the case with sound wall under all other input motions.

In a recent experimental study using the shake-table test, Wilson and Elgamal (2009) investigated the passive force-displacement and dynamic earth pressure on a bridge abutment. It was found that the modified M-O method, which included the effect of soil cohesion based on the model by Anderson *et al.* (2009), performed best with input motions of 0.66g or less. The pressure was underestimated with stronger input motions. None of the theoretical methods (Mononobe and Matsuo 1929, Seed and Whitman 1970, Kramer 1996) that were used for predicting the dynamic earth pressure resultant force were accurate for the full range of input motions in their study (Wilson 2009).

## 6. Conclusions

Full-scale shake table tests of two semi-gravity cantilever concrete retaining walls, with and without sound wall, were conducted on a large outdoor shake-table to investigate the performance of retaining walls under seismic loads. Both walls were backfilled with compacted soil on one side and supported on flexible foundation in a steel soil container fixed on the shake table. The soil-wall systems were then subjected to a series of unidirectional seismic excitations. The lateral movements of the walls, dynamic earth pressure, and behavior of the backfill soil were discussed and compared between the two tests. Based on the current study, the following main conclusions can be drawn:

- The primary damage observed during the tests was associated with the large lateral displacement of the retaining wall and cracking at the wall stem-footing joints. Slip planes were not directly measured in the backfills but could have formed based on the soil movement measured by the MEM sensors. No other structural damage or collapse occurred during the tests.
- Among the three earthquake motions, the earthquake input with much smaller acceleration (Kocaeli) introduced the least amount of dynamic response in the soil-wall systems tested here (where the retaining wall had a stem height of 1.83 m).
- For the test without sound wall, the dynamic pressure distribution behind the retaining wall displayed a nonlinear trend and the resultant of the pressure acted at a height of 0.4H in this test. Arching effect likely existed towards the bottom of the stem, resulting in small pressure values near the bottom of the wall. This was also observed in several other existing literatures.
- The pressure distribution indirectly obtained from strain gage readings did not include the local soil arching effect, thus giving a linear distribution. These results should be treated with caution.
- The retaining wall with sound wall behaved differently from the wall without sound wall. The dynamic pressure distribution exhibited a higher nonlinearity (polynomial shape). Reverse thrusting effect was found near the top of the stem, which introduced large pressure towards the top of the wall.
- Based on the comparison with the test results, the M-O method lacks sufficient accuracy in estimating the dynamic earth pressure behind walls under various earthquake input motions studied, especially for the retaining wall with sound wall. Further investigation is needed in the design implications of retaining walls using the existing M-O method.

## Acknowledgments

This research was supported by the California Department of Transportation (Caltrans) under the Grant No. 59A0650. The testing facility and the technical support provided by the National Science Foundation (NSF) George E. Brown, Jr. *Network for Earthquake Engineering Simulation Research* (*NEESR*) and the University of California, San Diego, are also greatly acknowledged.

## References


AASHTO (2005), *AASHTO LRFD Bridge Design Specifications* (3rd edn), AASHTO, Washington DC.

Aggour, M. and Brown, C. (1974), "The prediction of earth pressure on retaining walls due to compaction", *Geotech.*, **24**(4), 489-502.

Al Atik, L. and Sitar, N. (2007), *Development of Improved Procedures for Seismic Design of Buried and Partially Buried Structures*, Report No. 2007/06, Pacific Earthquake Engineering Research Center (PEER), University of California, Berkeley.

Anderson, D, Martin, G.R., Lam, I. and Wang, J.N. (2009), *Seismic Analysis and Design of Retaining Walls, Buried Structures, Slopes, and Embankments*, NCHRP Rep. 611, Transportation Research Board, Washington DC.

ASTM (2005a), *Standard Test Method for Compressive Strength of Cylindrical Concrete Specimens*, ASTM Standard C39/C39M, ASTM International, West Conshohocken, PA.

ASTM (2005b), *Standard Test Methods and Definitions for Mechanical Testing of Steel Products*, ASTM Standard A370, ASTM International, West Conshohocken, PA.

ASTM (2005c), *Standard Specification for Load Bearing Concrete Masonry Units*, ASTM Standard C90, ASTM International, West Conshohocken, PA.

ASTM (2005d), *Standard Specification for Mortar for Unit Masonry*, ASTM Standard C270, ASTM International, West Conshohocken, PA.

ASTM (2005e), *Standard Specification for Grout for Masonry*, ASTM Standard C476, ASTM International, West Conshohocken, PA.

ASTM (2005f), *Standard Test Method for Consolidated Undrained Triaxial Compression Test for Cohesive Soils*, ASTM Standard D4767, ASTM International, West Conshohocken, PA.

Bentler, J. and Labuz, J. (2006), "Performance of a cantilever retaining wall", *J. Geotech. Geoenvironmental Eng.*, **132**(8), 1062–1070.

Bolton, M. and Steedman, R.S. (1982), "Centrifugal testing of microconcrete retaining walls subjected to base shaking", *Soil Dynamics and Earthquake Engineering Conference*, Southampton, England, 311–329.

Bolton, M. and Steedman, R.S. (1985), "The behavior of fixed cantilever walls subjected to lateral shaking", *Proceedings of Symposium on the Application of Centrifuge Modeling to Geotechnical Design*, Balkema, Rotterdam, 302–314.

Caltrans (1999), *Standard Specifications*. The California Department of Transportation, Sacramento, CA.

Caltrans (2008), *Bridge Standard Detail Sheets*. The California Department of Transportation, CA. http://www.dot.ca.gov/hq/esc/techpubs/manual/bridgemanuals/bridge-standard-detail-sheets/, cited on April 17, 2012.

CDOT (2009), *Bridge Design Manual*, Colorado Department of Transportation, available at http://www.coloradodot.info/library/bridge/bridge-manuals/bridge-design-manual, cited on April 17, 2012.

Dewoolkar, M., Ko, H. and Pak, R. (2001), "Seismic behavior of cantilever retaining walls with liquefiable backfills", *J. Geotech. Geoenviron. Eng.*, **127**(5), 424-435.

Fang, Y. and Ishibashi, I. (1986), "Static earth pressures with various wall movements", *J. Geotech. Geoenviron. Eng.*, **112**(3), 317-333.

Fang, Y.S., Yang, Y.C. and Chen, T.J. (2003), "Retaining walls damaged in the Chi-Chi earthquake", *Can. Geotech. J.*, **40**(6), 1142–1153.

Gere, J.M. and Timoshenko, S.P. (1997), *Mechanics of Materials*, PWS Publishing Company.

Jung, C. and Bobet, A. (2008), "Seismic earth pressures behind retaining walls: effects of rigid body motions", *Proceedings of Geotechnical Earthquake Engineering and Soil Dynamics IV*, Sacramento, CA.

Koseki, J., Tatsuoka, F., Munaf, Y., Tateyama, M. and Kojima, K. (1998), "A modified procedure to evaluate active earth pressure at high seismic loads," *Soils and Foundations*, Special Issue on Geotechnical Aspects of the January 17 1995 Hyogoken-Nambu Earthquake, **2**, pp. 209–216.

Kramer, S. (1996), *Geotechnical Earthquake Engineering*, Prentice-Hall: Upper Saddle, NJ.

Kutter, B.L., Casey, J.A. and Romstad, K.M. (1990), "Centrifuge modeling and field observations of

dynamic behavior of reinforced soil and concrete cantilever retaining walls", *Proceedings of Fourth U.S. National Conference on Earthquake Engineering*, Palm Springs, CA, May 20–24, 663-672.
Ling, H.I. (2003), "A critical review of full-scale shaking table tests conducted on reinforced soil retaining walls", In *Reinforced Soil Engineering: Advances in Research and Practice*, Marcel Dekker, New York, 491-10.
Ling, H.I., Liu, H., Kaliakin, V.N. and Leshchinsky, D. (2004), "Analyzing dynamic behavior of geosynthetic-reinforced soil retaining walls", *J. Eng. Mech.*, **130**(8), 911-920.
Ling, H.I., Mohri, Y., Leshchinsky, D., Burke, C., Matsushima, K. and Liu, H. (2005), "Large-scale shaking table tests on modular-block reinforced soil retaining walls", *J. Geotech. Geoenviron. Eng.*, **131**(4), 465-476.
Mock, E. and Cheng, L. (2011), "Full-scale shake table test of retaining walls with and without sound wall," Test Report, CA/UCD-SESM-10-03, University of California, Davis, CA.
Mononobe, N. and Matsuo, H. (1929), "On the determination of earth pressures during earthquakes", *World Engineering Conference*, Tokyo, Japan, 177-185.
Mortezaei, A. and Zahrai, S.M. (2009), "Seismic response of reinforced concrete building with viscoelastic damper under near field earthquake", *Asian J. Civil Eng.* (Building and Housing), **9**(3), 347-359.
NEESR (2012), The George E. Brown, Jr. Network for Earthquake Engineering Simulation Research. Official website available at http://www.nees.org, cited on March 28, 2012.
Newmark, N. (1965), "Effects of earthquakes on dams and embankments", *Géotechnique*, **15**(2), 139-160.
Ortiz, L. (1982), "Dynamic centrifuge testing of cantilever retaining walls", Ph.D. Dissertation, California Institute of Technology, Pasadena, CA.
Ortiz, L., Scott, R. and Lee, J. (1983), "Dynamic centrifuge testing of a cantilever retaining wall", *Earthq. Eng. Struct. Dyn.*, **1**(2), 251-268.
Paik, K.H. and Salgado, R. (2003), "Estimation of active earth pressure against rigid retaining walls considering arching effects", *Géotech.*, **53**(7), 643-653.
PEER (2013), PEER Strong Motion Database, Pacific Earthquake Engineering Research Center, website available at http://peer.berkeley.edu/peer_ground_motion_database, cited on March 4, 2013.
Restrepo, J.I., Conte, J.P., Luco, J.E., Seible, F. and Van Den Einde, L. (2005), "The NEES@UCSD Large High Performance Outdoor Shake Table Earthquake Engineering and Soil Dynamics (GSP 133)", *Proceedings of the Geofrontiers Conference*, Austin, TX, January 24-26.
Richards, R. and Elms, D.G. (1979), "Seismic behavior of gravity retaining wall", *J. Geotech. Eng. Div.*, **105**(GT4), 449-464.
Seed, H.B. and Whitman, R.V. (1970), "Design of earth retaining structures for dynamic loads," State-of-the-Art Papers presented at the Special Conference: *Lateral Stresses in the Ground and Design of Earth-Retaining Structures*, Ithaca, NY, June 22–24, pp. 103-147.
Siddharthan, R.V., Ganeshwara, V., Kutter, B.L., El-Desouky, M. and Whitman, R.V. (2004), "Seismic deformation of bar mat mechanically stabilized earth walls. I: centrifuge tests", *J. Geotech. Geoenviron. Eng.*, **130**(1), 14-25.
Stadler, A.T. (1996) "Static and dynamic behavior of cantilever retaining walls", Ph.D. Dissertation, University of Colorado at Boulder, Boulder, CO.
Tajiri, N., Sasaki, H., Nishimura, J., Ochiai, Y. and Dobashi, K. (1996), "Full-scale failure experiments of geotextile-reinforced soil walls with different facings", in *Earth Reinforcement*, Ed. H. Ochiai *et al.*, Balkema, Rotterdam, The Netherlands, 525-530.
Tavatli, D. and Li, J. (2007), "Seismic analysis of semi-gravity retaining wall", Power Point Presentation, The California Department of Transportation, Sacramento, CA.
US Army Corps of Engineers (2012), "Appendix G – Earthquake forces from backfill", Stability Analysis of Concrete Structures, Engineer Manuals, EM 1110-2-2100, available at http://140.194.76.129/publications/eng-manuals/EM_1110-2-2100_sec/Sections/a-g.pdf, cited on March 4, 2013.
Wilson, P. (2009), "Large scale passive force-displacement and dynamic earth pressure experiments and

simulations", Ph.D. Dissertation, University of California, San Diego, San Diego, CA.
Wilson, P. and Elgamal, A. (2009), "Full-scale shake table investigation of bridge abutment lateral earth pressure", *Bull. New Zealand Soc. Earthq. Eng.* (NZSEE), **42**(1), 39-46.
Yagi, Y. and Kikuchi, M. (2000), "Source rupture process of the Kocaeli, Turkey, earthquake of August 17, 1999, obtained by joint inversion of near-field data and teleseismic data", *Geophy. Res. Lett.*, **27**(13), 1969-972.

*JL*